LETTER

Observations of increased tropical rainfall preceded by air passage over forests

D. V. Spracklen[1], S. R. Arnold[1] & C. M. Taylor[2]

Vegetation affects precipitation patterns by mediating moisture, energy and trace-gas fluxes between the surface and atmosphere[1]. When forests are replaced by pasture or crops, evapotranspiration of moisture from soil and vegetation is often diminished, leading to reduced atmospheric humidity and potentially suppressing precipitation[2,3]. Climate models predict that large-scale tropical deforestation causes reduced regional precipitation[4–10], although the magnitude of the effect is model[9,11] and resolution[8] dependent. In contrast, observational studies have linked deforestation to increased precipitation locally[12–14] but have been unable to explore the impact of large-scale deforestation. Here we use satellite remote-sensing data of tropical precipitation and vegetation, combined with simulated atmospheric transport patterns, to assess the pan-tropical effect of forests on tropical rainfall. We find that for more than 60 per cent of the tropical land surface (latitudes 30 degrees south to 30 degrees north), air that has passed over extensive vegetation in the preceding few days produces at least twice as much rain as air that has passed over little vegetation. We demonstrate that this empirical correlation is consistent with evapotranspiration maintaining atmospheric moisture in air that passes over extensive vegetation. We combine these empirical relationships with current trends of Amazonian deforestation to estimate reductions of 12 and 21 per cent in wet-season and dry-season precipitation respectively across the Amazon basin by 2050, due to less-efficient moisture recycling. Our observation-based results complement similar estimates from climate models[4–10], in which the physical mechanisms and feedbacks at work could be explored in more detail.

To explore the links between vegetation and rainfall, we analysed combined satellite data on precipitation from the Tropical Rainfall Measuring Mission (TRMM) and other satellites[15] (TRMM3B42) and data on leaf area index (LAI) from the Moderate Resolution Imaging Spectroradiometer[16] (MODIS). In these data positive spatial correlations exist between annual mean precipitation and annual mean LAI (Fig. 1a, d; Pearson correlation coefficient, $r = 0.81$), highlighting the role of precipitation in controlling large-scale vegetation patterns. In this study, our aim was to investigate a causal effect of vegetation on tropical ($30°$ S to $30°$ N) rainfall in subsequent days on a regional scale (over distances of hundreds to thousands of kilometres). To do this, we calculated the origin and atmospheric transport of air
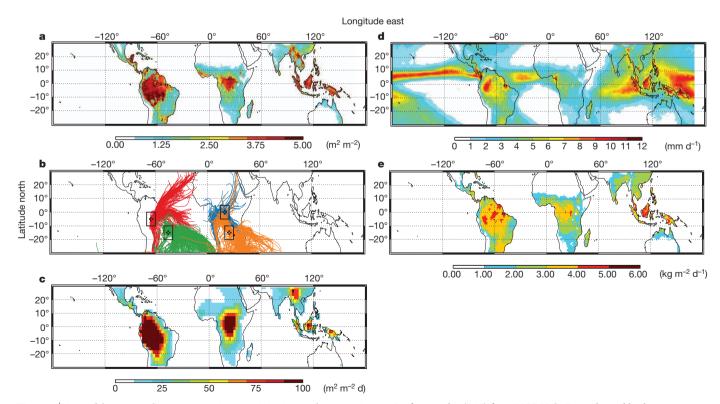

Figure 1 | Annual (2001–2007) mean vegetation, precipitation and evaporation. a, Leaf area index (LAI) from MODIS. b, Example 10-d back-trajectories arriving daily during 2001. Boxes illustrate the four domains analysed in detail in this study. c, Mean cumulative exposure of back-trajectories to LAI over the preceding 10 d. d, Precipitation reported by TRMM and other satellites (TRMM3B42). e, Evapotranspiration computed as the mean of the four GLDAS models.

[1]School of Earth and Environment, University of Leeds, Leeds LS2 9JT, UK. [2]Centre for Ecology and Hydrology, Wallingford, Oxford OX10 8BB, UK.

masses to determine the prior exposure of air to vegetation. This allowed us to evaluate whether air that had passed over more vegetation produced more rainfall.

To calculate air-mass histories, we used a Lagrangian atmospheric transport model. Such back-trajectory methods have been used previously to identify the transport of atmospheric moisture to continental regions[17,18]. We calculated atmospheric back-trajectories arriving daily at the centre of all continental $1° \times 1°$ grid squares over the tropical domain for 2001–2007. The trajectories were calculated using operational analysis data from the European Centre for Medium-Range Weather Forecasts (ECMWF), and are hence consistent with the large-scale atmospheric flow from the assimilated observations. We tested the sensitivity of our analysis to the length, arrival height and arrival time of the back-trajectories and found consistent results across a broad range of choices (Supplementary Figs 1, 2 and 3). Here we present results for ten-day back-trajectories arriving at the surface at 12:00 UT. Figure 1b shows example back-trajectories arriving at four tropical locations.

For each individual trajectory, we calculated the cumulative LAI (ΣLAI) encountered by the air mass during the last ten days of atmospheric transport. The resulting climatology of ΣLAI (Fig. 1c) is very similar to the *in situ* LAI, although important differences are apparent. For example, there are regions surrounding the Amazon and Congo basins where *in situ* LAI is relatively low but ΣLAI is high owing to exposure of air to large amounts of vegetation as it travels across forested regions upwind.

We analysed relationships between the daily variability in ΣLAI and the daily variability in precipitation. Figure 2a shows these relationships for air masses arriving in a ~1,000 km × 1,000 km region of Minas Gerais, Brazil, near the Amazon basin. To reduce the influence of the initial state of the air mass on our analysis, we stratified the data into that from the wet season and that from the dry season and then further according to the initial specific humidity of the trajectory, on the basis of the ECMWF analyses. We found a strong positive and significant (Student's *t*-test, $P < 0.01$) relationship between the exposure of air masses to vegetation and the precipitation those air masses produce (Fig. 2b). For air masses with low to medium exposure to precedent vegetation (ΣLAI $< 10\,m^2\,m^{-2}$ d), mean dry- and wet-season rainfall increases by 0.25 mm d^{-1} and, respectively, 0.4 mm d^{-1} for every additional unit of exposure to LAI that is encountered in the preceding 10 d. The impact of vegetation exposure tends to saturate, especially during the wet season, with less sensitivity of rainfall where ΣLAI $> 10\,m^2\,m^{-2}$ d. Although we find that the initial specific humidity of the air mass does affect precipitation, with moister air masses typically producing more precipitation, the positive trend between precipitation and exposure to LAI is similar for all subsets of the data. Qualitatively similar results are found in a 1,000 km × 1,000 km region south of the tropical forests of the Congo basin (Fig. 2b). Over the moist tropical forests themselves, differences in rainfall between air masses with low and high exposures to LAI are notably smaller (Fig. 2b), although for the Congo basin the differences are significant in the dry season ($P < 0.01$). We note that the positive relationships found between precipitation and ΣLAI are not due to the length of time the trajectories have spent over land, with distance travelled and ΣLAI often poorly correlated (Supplementary Table 1), or to the average topographic height the trajectory has crossed. When we repeated our analysis using the distance travelled by the trajectory over land or the average elevation of the topography crossed by the trajectory (in place of ΣLAI), the relationships were substantially weaker and in some cases negative (Supplementary Figs 4 and 5).

We extended this regional analysis to explore relationships between precipitation and vegetation across the tropics (Fig. 2c). For more than 60% of the tropical land surface, precipitation is a factor of at least two greater in air masses that have been exposed to extensive vegetation in the preceding days (defined as the top decile of ΣLAI), relative to air masses that have been exposed to little (defined as the bottom decile of
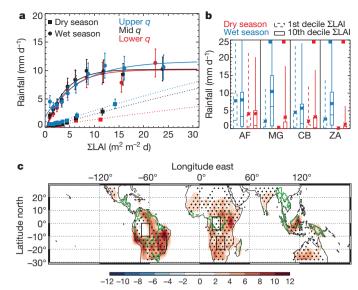

Figure 2 | Relationships between daily precipitation and cumulative exposure of 10-d back-trajectories to vegetation LAI (ΣLAI) for 2001–2007. a, Plot for air masses arriving in Minas Gerais, Brazil (10–20° S, 40–50° W). Data binned into deciles of ΣLAI and stratified by initial specific humidity (*q*). Lines show fit to data (solid, wet season; dotted, dry season) and error bars indicate estimation of error in precipitation (Methods Summary). **b**, Comparison of daily precipitation for air masses that have been exposed to small and large amounts of vegetation (significant ($P < 0.01$) differences indicated by squares at top of panel) during atmospheric transport to the Amazon basin (AB; 10–0° S, 60–70° W), Minas Gerais (MG; 10–20° S, 40–50° W), the Congo basin (CB; 5° N–5° S, 15–25° E) and south of Congo (ZA; 10–20° S, 20–30° E) (mean, star; median, line; 25th and 75th percentiles, box; 5th and 95th percentiles, whiskers). **c**, Number of calendar months with significant ($P < 0.01$; red, positive; blue, negative) relationships between precipitation and ΣLAI. Stippling denotes regions where precipitation is a factor of at least two greater in air with large exposure to vegetation than in air with small exposure. Green contour delimits areas with >3 m^2 m^{-2} annual mean LAI. Black boxes mark the four regions in **b**.

ΣLAI). Significant ($P < 0.01$) positive correlations between precipitation and ΣLAI are common features for much of the year in areas surrounding the Amazon (southern Brazil and Paraguay) and Congo (southern and eastern Africa) forests, matching where previous studies have found large continental precipitation recycling ratios[18]. We find few tropical regions with significant negative correlations, although the relationships between vegetation and precipitation are typically weaker in moist tropical forests. The weaker signal at the centre of extensive forests is probably due to the lack of variability in air-mass exposure to vegetation (Supplementary Fig. 6); however, saturation of the MODIS LAI retrievals for dense tropical forest canopies[19] may have a role.

This analysis demonstrates that there are strong positive relationships between the cumulative exposure of air to vegetation and the amount of precipitation that air will produce, suggestive of a water-cycle feedback. To explore potential mechanisms underlying these relationships, we evaluated the change in atmospheric moisture that occurs along our back-trajectories. To do this we calculated the net change in specific humidity (Δq) that occurred during continental transport in the ECMWF humidity analyses along the 10-d back-trajectories (Fig. 3a). In general, air becomes drier during atmospheric transport over land, owing to lower continental evaporation rates as compared with the oceans. Figure 3a demonstrates that air masses that have been exposed to more vegetation remain significantly moister ($P < 0.01$), and in some cases air can actually moisten when crossing densely vegetated regions. Analysis of the latter cases indicates that typically 70–90% of increases in *q* occur during the hours of daylight,
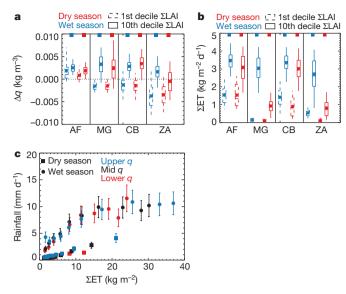
Figure 3 | Atmospheric water-budget components along back-trajectories.
a, Same as Fig. 2b, but for net change in atmospheric specific humidity (Δq) as a function of ΣLAI. **b**, Same as Fig. 2b, but for cumulative surface evaporation (ΣET) as a function of ΣLAI. **c**, Same as Fig. 2a, but for precipitation as a function of ΣET.

Figure 4 | Simulated percentage change in precipitation due to 2000–2050 business-as-usual deforestation of the Amazon basin. a, Wet season; **b**, dry season. Stippling denotes regions where the simulated precipitation anomaly differs from the present-day (1998–2010) rainfall by more than 1 s.d. The Amazon (black) and Rio de la Plata (red) basins are marked.

consistent with a dominant forcing from evapotranspiration (Supplementary Fig. 7).

To quantify the contribution of evapotranspiration to the air-mass water budget, we used output from four global land surface models that use the best available estimates of meteorological forcing (those from the Global Land Data Assimilation System[20] (GLDAS)) (Fig. 1e). Figure 3b shows significant ($P < 0.01$) positive relationships between the multi-model mean cumulative surface evaporation (ΣET) and ΣLAI in all four regions examined. Figure 3c shows rainfall as a function of ΣET for the Minas Gerais region, demonstrating that additional moisture from evapotranspiration emitted into air masses with large exposure to vegetation is substantially greater than the additional precipitation observed in these air masses. Indeed, for all four regions the extra ΣET emitted into air masses with large vegetation exposure exceeds the observed additional precipitation by a factor of at least four (Supplementary Table 2).

Our analysis explores the role of regional-scale vegetation patterns on precipitation. Through evapotranspiration, forests maintain atmospheric moisture that can return to land as rainfall downwind. These processes operate on timescales of days over distances of 100–1,000 km (ref. 18) such that large-scale land-use change may alter precipitation hundreds to thousands of kilometres from the region of vegetation change. Land-use patterns and small-scale deforestation may also alter precipitation locally, through changes in the thermodynamic profile and the development of surface-induced mesoscale circulations[21,22]. Natural and pyrogenic emissions from vegetation can also have a role in rainfall initiation over tropical forest regions[23]. The impact of cloud microphysical processes on precipitation is highly uncertain[24], and biogenic emissions could contribute to our observed relationship between rainfall and exposed vegetation. However, our water-balance calculations imply that cumulative increases in evapotranspiration over upstream forested regions more than account for the increase in downstream rainfall.

Rapid land-use change is occurring across large regions of the tropics: 40% of the Amazon is predicted to be deforested by 2050 under a business-as-usual scenario[25]. We used this scenario to explore the potential sensitivity of rainfall to changes in moisture recycling as a result of deforestation. We combined the deforestation scenario with present-day LAI to produce a new spatial distribution of LAI
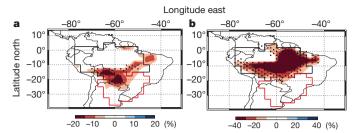
(Supplementary Fig. 8) and then used our trajectories to calculate ΣLAI under the deforested scenario. We then applied our empirical relationships between ΣLAI and rainfall (Fig. 2b) to estimate the change in rainfall that might occur as a result of this extensive deforestation. In this calculation, we implicitly assumed there to be no change in the large-scale circulation and that the local effects of deforestation on rainfall were negligible downstream. Despite these assumptions, our estimates are broadly consistent with estimates of basin-wide deforestation from climate models[4–10]. Using this method, we estimated a 12% reduction in wet-season precipitation and a 21% reduction in dry-season precipitation across the Amazon basin (Fig. 4). This sensitivity is not restricted to the region of deforestation, and we estimate a 4% decrease in annual total precipitation for the Rio de la Plata basin. Through comparison with TRMM3B42 data, we calculate that the estimated reduction in precipitation is equivalent to the basin-wide drought experienced across the Amazon in 2010. Such a reduction in precipitation may have consequences for the future of remaining Amazonian forests[26,27] and for rainfall-reliant industries both within and outside the Amazon basin, including agriculture and hydroelectric power generation, which contribute substantially to South American economies. The successful efforts to curb Amazon deforestation that have been applied in recent years[28] must be maintained if large-scale clearance of the Amazon and the resulting impacts on regional rainfall are to be avoided.

METHODS SUMMARY

Remote-sensed data. We used precipitation retrievals from the 3B42 3-h 0.25° × 0.25° product of TRMM and other satellites[15] to calculate daily accumulated (24-h) rainfall. We used monthly mean LAI from MODIS[16] using the MOD15_BU_V5 product available at 0.25° × 0.25° resolution. We spatially averaged both products to 1° × 1° resolution. We apply this temporal and spatial averaging to the precipitation data to reduce random error[29]. We estimate the total error to be the random error, estimated according to ref. 28, plus a systematic error estimated as 0.2 times the absolute precipitation[30], combined in quadrature.

Land surface models. We used 1° × 1° monthly mean evaporation from four global land surface models archived on GLDAS[20]. The models are forced by a combination of meteorological data sets including atmospheric analysis, and precipitation from merged gauge–satellite products.

Atmospheric transport. We calculated kinematic atmospheric back-trajectories arriving four times daily (00:00, 06:00, 12:00 and 18:00 UT) on a 1° × 1° grid for the period 2001–2007 using the OFFLINE trajectory model. The position of each trajectory is calculated every 30 min and output every 6 h. We calculated 3-, 5- and 10-d trajectories arriving at the surface and three altitudes above the surface (corresponding to air pressures of 900, 800 and 700 hPa) that are likely to be within the deep tropical boundary layer.

Analysis. For each trajectory, we calculated the total distance travelled over land, the cumulative exposure to LAI (ΣLAI), the average elevation of the topography over which the trajectory travelled and the cumulative evapotranspiration (ΣET; specified by GLDAS). We fitted rainfall data with a function of the form $f(x) = ae^{bx} + c$ (Supplementary Table 2). We calculated ΣLAI regardless of trajectory pressure. Restricting the calculation to when trajectory pressure is greater than 850 hPa gives similar results (Supplementary Fig. 9).

1. Bonan, G. B. Forests and climate change: forcings, feedbacks, and the climate benefit of forests. *Science* **320,** 1444–1449 (2008).
2. Shukla, J. & Mintz, Y. Influence of land-surface evapotranspiration on the Earth's climate. *Science* **215,** 1498–1501 (1982).
3. Eltahir, E. A. B. & Bras, R. L. Precipitation recycling in the Amazon basin. *Q. J. R. Meteorol. Soc.* **120,** 861–880 (1994).
4. Henderson-Sellers, A. & Gornitz, V. Possible climatic impacts of land cover transformations, with particular emphasis on tropical deforestation. *Clim. Change* **6,** 231–257 (1984).
5. Lean, J. & Warrilow, D. A. Simulation of the regional climatic impact of Amazon deforestation. *Nature* **342,** 411–413 (1989).
6. Shukla, J., Nobre, C. & Sellers, P. Amazon deforestation and climate change. *Science* **247,** 1322–1325 (1990).
7. Werth, D. & Avissar, R. The local and global effects of Amazon deforestation. *J. Geophys. Res.* **107,** 8087 (2002).
8. Ramos da Silva, R., Werth, D. & Avissar, R. Regional impacts of future land-cover changes on the Amazon basin wet-season climate. *J. Clim.* **21,** 1153–1170 (2008).
9. Hasler, N., Werth, D. & Avissar, R. Effects of tropical deforestation on global hydroclimate: a multimodel ensemble analysis. *J. Clim.* **22,** 1124–1141 (2009).
10. Nobre, P. *et al.* Amazon deforestation and climate change in a coupled model simulation. *J. Clim.* **22,** 5686–5697 (2009).
11. Pitman, A. J. *et al.* Uncertainties in climate responses to past land cover change: first results from the LUCID intercomparison study. *Geophys. Res. Lett.* **36,** L14814 (2009).
12. Butt, N., de Oliveira, P. A. & Costa, M. H. Evidence that deforestation affects the onset of the rainy season in Rondonia, Brazil. *J. Geophys. Res.* **116,** D11120 (2011).
13. Negri, A. J., Adler, R. F., Xu, L. & Surratt, J. The impact of Amazonian deforestation on dry season rainfall. *J. Clim.* **17,** 1306–1319 (2004).
14. Chagnon, F. J. F. & Bras, R. L. Contemporary climate change in the Amazon. *Geophys. Res. Lett.* **32,** L13703 (2005).
15. Huffman, G. *et al.* The TRMM multisatellite precipitation analysis (TMPA): quasi-global, multiyear, combined-sensor precipitation estimates at fine scales. *J. Hydrometeorol.* **8,** 38–55 (2007).
16. Myneni, R. B. *et al.* Global products of vegetation leaf area index and fraction absorbed PAR from year one of MODIS data. *Remote Sens. Environ.* **83,** 214–231 (2002).
17. Gimeno, L., Drumond, A., Nieto, R., Trigo, R. M. & Stohl, A. On the origin of continental precipitation. *Geophys. Res. Lett.* **37,** L13804 (2010).
18. van der Ent, R. J., Savenije, H. H. G., Schaefli, B. & Steele-Dunne, S. C. Origin and fate of atmospheric moisture over continents. *Wat. Resour. Res.* **46,** W09525 (2010).
19. Aragão, L. E. O. C. *et al.* Spatial validation of collection 4 MODIS LAI product in eastern Amazonia. *IEEE Trans. Geosci. Rem. Sens.* **43,** 2526–2534 (2005).
20. Rodell, M. *et al.* The global land data assimilation system. *Bull. Am. Meteorol. Soc.* **85,** 381–394 (2004).
21. Wang, J. F., Bras, R. L. & Eltahir, E. A. B. The impact of observed deforestation on the mesoscale distribution of rainfall and clouds in Amazonia. *J. Hydrometeorol.* **1,** 267–286 (2000).
22. Garcia-Carreras, L. & Parker, D. J. How does local tropical deforestation affect rainfall? *Geophys. Res. Lett.* **38,** L19802 (2011).
23. Andreae, M. O. *et al.* Smoking rain clouds over the Amazon. *Science* **303,** 1337–1342 (2004).
24. Koren, I. *et al.* Aerosol-induced intensification of rain from the tropics to mid-latitudes. *Nature Geosci.* **5,** 118–122 (2012).
25. Soares-Fihlo, B. S. *et al.* Modelling conservation in the Amazon basin. *Nature* **440,** 520–523 (2006).
26. Phillips, O. L. *et al.* Drought sensitivity of the Amazon rainforest. *Science* **323,** 1344–1347 (2009).
27. Aragão, L. E. O. C. *et al.* Spatial patterns and fire response of recent Amazonian droughts. *Geophys. Res. Lett.* **34,** L07701 (2007).
28. Davidson, E. A. *et al.* The Amazon basin in transition. *Nature* **481,** 321–328 (2012).
29. Huffman, G. J. Estimates of root-mean-square random error for finite samples of estimated precipitation. *J. Appl. Meteorol.* **36,** 1191–1201 (1997).
30. Smith, T. M., Arkin, P. A., Bates, J. J. & Huffman, G. J. Estimating bias of satellite precipitation estimates. *J. Hydrometeorol.* **7,** 841–856 (2006).

METHODS

Remote-sensed data. We used precipitation retrievals (from the Tropical Rainfall Measuring Mission (TRMM; http://trmm.gsfc.nasa.gov/) and other satellites) in the 3B42 3-h $0.25° \times 0.25°$ product[15] to calculate daily accumulated (24 h) rainfall. This product reports precipitation from microwave sensors on board polar-orbiting satellites, combined with more frequent cloud-top temperature data, surface rain gauge analysis and the precipitation radar on TRMM. We used the monthly mean leaf area index (LAI) from the Moderate Resolution Imaging Spectroradiometer (MODIS; http://modis.gsfc.nasa.gov/data/dataprod/dataproducts.php?MOD_NUMBER=15)[16] using the MOD15_BU_V5 product available at $0.25° \times 0.25°$ resolution.

The precipitation product includes both systematic and random error[29,30]. Systematic biases of $0.5–1\,\mathrm{mm\,d^{-1}}$, or 0.2 times the mean precipitation, have been estimated[30]. To reduce the random error we spatially averaged the precipitation product to $1° \times 1°$ resolution and temporally averaged to give daily accumulated (24 h) precipitation. This temporal and spatial averaging applied to TRMM3B42 means that each data point in our analysis (which corresponds to a single trajectory) is the average of 128 TRMM3B42 data points. This substantially reduces the random error that is present in the TRMM3B42 product[29]. We estimate the random error using the method of ref. 29 and assume a systematic error of 0.2 times the mean precipitation[30]. We combine the random and systematic errors in quadrature to give an estimate of the total error, which in any case is substantially smaller than the large effect of vegetation on precipitation. We spatially averaged the LAI data to the same resolution as the precipitation product.

Land surface models. We used $1° \times 1°$ monthly mean evaporation from four global land surface models (Community Land Model (CLM), Variable Infiltration Capacity model (VIC), NOAH and MOSIAC) archived on the Global Land Data Assimilation System (GLDAS; http://disc.sci.gsfc.nasa.gov/services/grads-gds/gldas)[20]. The models are forced by a combination of meteorological data sets including atmospheric analysis, and precipitation from merged gauge–satellite products.

Atmospheric transport. We calculated kinematic atmospheric back-trajectories arriving daily (00:00, 06:00, 12:00 and 18:00 UT) on a $1° \times 1°$ grid for the period 2001–07 using the OFFLINE trajectory model[31]. The position of each trajectory is calculated every 30 min, and output every 6 h. We calculated 3-, 5- and 10-day trajectories arriving at the surface and 3 levels above the surface (900, 800 and 700 hPa) that are likely to be within the deep tropical boundary layer. We demonstrate that our results are robust to the back-trajectory length (Supplementary Fig. 1), arrival pressure (Supplementary Fig. 2) and arrival time (Supplementary Fig. 3) of the trajectory. Throughout the Letter we report analysis of 10-day back-trajectories arriving at the surface at 12:00 UT.

Analysis. For each trajectory we calculated (1) total distance travelled over land (Σdist), (2) cumulative exposure to LAI (ΣLAI), (3) average elevation of the topography (specified by the Climate Research Unit CRU CL 2.0 database, 10′ resolution) over which the air mass travels, and (4) cumulative evapotranspiration (specified by GLDAS; ΣET). We calculate ΣLAI regardless of trajectory pressure but show that restricting the calculation to when trajectory pressure is greater than 850 hPa gives similar results (Supplementary Fig. 9).

We analysed relationships between daily precipitation and the variables calculated from air mass history (Σdist, ΣLAI and ΣET). We stratified trajectories into dry season and wet season and according to the initial specific humidity (q) of the back-trajectory (taken from the ECMWF analyses). The timings of wet and dry season are location dependent. For the purpose of this analysis we defined the dry season at any location as calendar months with below annual average precipitation for that location and the wet season as calendar months with above average precipitation (as observed by TRMM3B42; Supplementary Table 2). We demonstrated that this stratification results in large variability in initial q of the back-trajectory (Supplementary Table 2). We conducted detailed analysis over 4 large ($10° \times 10°$, ~1,000 km × 1,000 km) domains. Our pan-tropical analysis was conducted at a horizontal resolution of $2.5° \times 2.5°$. For our 7-year analysis each $10° \times 10°$ grid box represents 255,000 trajectories whereas each $2.5° \times 2.5°$ grid box represents 15,968 trajectories.

We binned trajectories into deciles of ΣLAI. We then compared back-trajectories with small exposure to vegetation (lowest decile of ΣLAI) to back-trajectories with large exposure to vegetation (largest decile of ΣLAI) and used the Student's t-test to determine the significance of any differences. Accounting for the stratification described above means that each data point (for example, data point in Fig. 2a, box-plot in Fig. 2b) represents 3,650 trajectories. We fitted relationships between precipitation and ΣLAI with functions of the form $y(x) = a\exp(bx) + c$ (see Fig. 2a). Supplementary Table 2 gives the fitted variables for the $10° \times 10°$ domains. Using a linear fit ($y(x) = ax + c$), which does not capture the nonlinear behaviour of the data well, altered our estimated impacts of deforestation on annual mean Amazon basin rainfall from −14% to −10%.

To estimate the impact of Amazonian deforestation on precipitation we combined the functions we fitted above with projected LAI distributions after deforestation. We created an LAI distribution for the year 2050 (see Supplementary Fig. 8) by combining a business-as-usual deforestation scenario[25] with the present-day LAI distribution from MODIS. We assumed that deforested areas are maintained as pasture with a LAI of $1\,\mathrm{m^2\,m^{-2}}$ (ref. 32). We then ran our present-day trajectories over the projected LAI to calculate the ΣLAI that would occur in the deforestation scenario. We used our empirical relationships (calculated at a resolution of $2.5° \times 2.5°$) along with ΣLAI to estimate the rainfall that would occur after deforestation. We estimated both wet season and dry season rainfall. Our approach only estimates the change in rainfall due to changes in water recycling. It makes the implicit assumption that there is no change in the large-scale circulation, and that the local impacts of deforestation on rainfall are negligible downstream. Calculation of the full impacts of deforestation on rainfall would require a climate model.

We compared the estimated changes in rainfall due to deforestation with present-day (1998–2010) rainfall recorded by TRMM3B42. We make comparisons for both the wet season and the dry season.

31. Methven, J. *Offline Trajectories: Calculation and Accuracy* Technical Report 44, (UK Universities Global Atmospheric Modelling Programme, University of Reading, 1997).
32. Aragão, L. E. O. C., Shimabukuro, Y. E., Santo, F. D. B. E. & Williams, M. Landscape pattern and spatial variability of leaf area index in Eastern Amazonia. *For. Ecol. Mgmt.* **211,** 240–256 (2005).